INVESTIGATION OF THERMAL DEGRADATION AND STABILITY IN MULTI-ALKALI ANTIMONIDE PHOTOCATHODES: NaKSb(Cs) vs KCsSb

S.K. Mohanty*[1,2], A. Oppelt[1], D. Sertore[2], F. Stephan[1], L. Monaco[2], M. Krasilnikov[1]
[1]DESY, Zeuthen, Germany
[2]Istituto Nazionale di Fisica Nucleare - LASA, Segrate, Italy

Abstract

Multi-alkali antimonide photocathodes have emerged as promising photoemissive materials for electron sources in high-repetition-rate free-electron laser (FEL) applications due to their low thermal emittance and high quantum efficiency in the green wavelength region. To evaluate their feasibility for operation in high-gradient RF guns, a collaborative effort between DESY-PITZ and INFN-LASA was initiated to develop and characterize multi-alkali photocathode materials under operative condition. As part of this effort, a NaKSb(Cs) photocathode belonging to the multi-alkali antimonide family was grown on a molybdenum substrate using a sequential deposition method in the new preparation system at INFN-LASA. A thermal degradation study of this photocathode was conducted, and its behavior was compared with a KCsSb film. This contribution presents the experimental results of the NaKSb(Cs) photocathode, focusing on its thermal degradation behavior and comparative analysis with the KCsSb photocathode.

INTRODUCTION

Alkali-based photocathodes with high quantum efficiency (QE) in the visible spectrum are attractive candidates for producing high-quality electron beams, making them well suited for applications in X-ray free-electron lasers (XFELs) and energy-recovery linacs (ERLs) [1]. However, despite their favorable photoemission properties, these materials are known to experience rapid QE degradation during operation in RF guns. Several studies, including our own operational experience, have reported a relatively short operational lifetime of these photocathodes [2–4]. Multiple factors contribute to this degradation, including chemical poisoning from residual gases, ion back-bombardment, laser-induced heating, and thermal decomposition of the photocathode material. Among these, thermal decomposition, driven by the photocathode operating temperature, may play a significant role in determining the photocathode's operational lifetime. During RF gun operation, the RF power dissipated in the cavity walls leads to heating of the gun structure and cathode region. Even with an efficient water-cooling system, the temperature may rise by tens of degrees Celsius above room temperature [5]. Therefore, investigating the performance and stability of alkali antimonide photocathodes at elevated temperatures is essential for understanding their degradation mechanisms and estimating their operational lifetime in RF gun environments.

* sandeep.mohanty@desy.de

Within the alkali antimonide family, two photocathodes—NaKSb(Cs) and KCsSb—were selected to investigate their degradation behavior at elevated temperatures, as they represent widely studied and comparatively robust members of the alkali antimonide photocathode family. The following section presents the growth recipe of the NaKSb(Cs) photocathode and discusses its thermal degradation characteristics, along with a comparison to the KCsSb photocathode.

PHOTOCATHODE PREPARATION

As reported in previous papers, a reproducible recipe for NaKSb(Cs) photocathodes has been established in our R&D preparation system at INFN LASA [6]. Encouraged by these positive results, we recently produced a NaKSb(Cs) photocathode using INFN-designed Mo plugs in a newly developed production chamber. A detailed description of the new production system can be found in references [2, 6–8].

One Mo plug was polished to a mirror-like finish (reflectivity > 54% at 543 nm, compared to the theoretical value of 57% [9]) to enable reflectivity measurements during and after the photocathode growth process. The sample was ultrasonically cleaned before being loaded into the UHV system. Prior to deposition, the cathode plug was heated to 450 °C for at least two to three hours to remove residual contaminants from the surface.

To better investigate the real-time photoemissive and optical properties during film deposition, a multi-wavelength diagnostic setup was implemented. This setup mainly consists of a Laser-Driven Light Source (LDLS) system and a motorized filter wheel. The filter wheel can accommodate up to eight different optical filters (254, 297, 365, 488, 515, 540, 632, and 690 nm) and rotates in a programmed sequence during deposition, enabling real-time monitoring of the photocurrent and reflectivity of the deposited films [7, 8]. For post-production optical characterization, a monochromator in combination with the LDLS light source is used.

RESULTS AND DISCUSSIONS

For the NaKSb(Cs)-1 cathode, the growth process was initiated by depositing a 5 nm thick Sb layer at 90 °C, followed by K and Na deposition at 110 °C until the photocurrent reached its maximum value. Subsequently, to enhance the final QE, Sb and Cs were further deposited in a yo-yo deposition sequence at 110 °C until the photocurrent approached saturation. All thicknesses mentioned above were measured using a Quartz Crystal Microbalance (QCM). The QE at 515 nm was recorded as 3.7% immediately after production. After deposition, the spectral response was measured and

is shown in Fig. 1. Analysis of the spectral response curve allowed us to estimate the value of $E_g + E_a$ (energy gap + electron affinity) of the photocathode, which represents the photoemission threshold in semiconductor photoemitters. The QE dependence near the photon energy threshold can be described using Eq. (1), originally reported by W. E. Spicer [10].

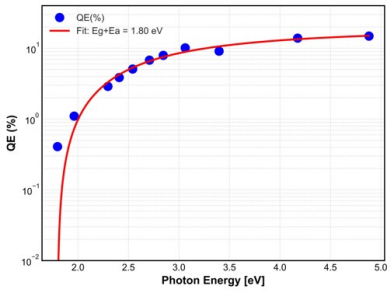

Figure 1: Spectral response of the NaKSb(Cs) photocathode (blue markers). The red curve represents the fit to the experimental data using Eq. (1).

$$QE = \frac{G(h\nu)\,[h\nu - (E_g + E_a)]^{1.5}}{[h\nu - (E_g + E_a)]^{1.5} + \gamma} \qquad (1)$$

In Eq. (1), $h\nu$ is the photon energy, $E_g + E_a$ represents the sum of the band gap and the electron affinity of the photocathode, and $G(h\nu)$ can usually be treated as a constant over the relevant photon energy range, as commonly assumed in the Spicer model [10]. The parameter γ is given by $\gamma = (\alpha + \beta)/C$, where β and C are constants and α is the absorption coefficient. By fitting Spicer's model (Eq. (1)) to the experimental data shown in Fig. 1, the photoemission threshold of the NaKSb(Cs) film was estimated to be 1.8 eV.

A comparison of the spectral response of the KCsSb cathode (cathode 137.3, Sb = 5 nm, thin KCsSb) and the NaKSb(Cs)-2 photocathode is shown in Fig. 2. For comparison, a thin KCsSb photocathode was used, as a similar Sb thickness was employed as the initial layer during the growth of the NaKSb(Cs) cathode. The detailed growth procedure of the thin KCsSb cathode (cathode 137.3) can be found in Ref. [8]. The spectral response comparison shown in Fig. 2 indicates improved QE at longer wavelengths for the NaKSb(Cs) photocathode compared to KCsSb, particularly in response to red laser light. This behavior may be attributed to the incorporation of Cs and Sb into the NaKSb bulk during the final stage of deposition, which likely reduces the overall electron affinity of the photocathode material [10–12].

Lifetime measurements were subsequently performed on the NaKSb(Cs) and KCsSb photocathodes (cathode 137.3, Sb = 5 nm, thin KCsSb) at different substrate temperatures in the new photocathode preparation system. Both photocathodes were subjected to an identical procedure, in which they were heated to different temperatures and maintained at each temperature for a defined duration to investigate QE degradation. During this process, the photocathodes were continuously illuminated with a green laser (540 nm), and the QE was measured in real time. Figure 3 illustrates the

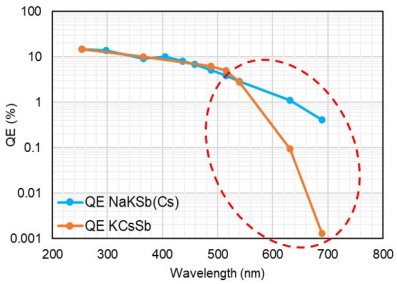

Figure 2: Comparison of the spectral response between the NaKSb(Cs) and KCsSb (thin, cathode 137.3) photocathodes. The difference in QE at longer wavelengths is highlighted by the circled region.

decay curves of the NaKSb(Cs) and KCsSb photocathodes at different substrate temperatures, with the initial QE normalized to unity. As observed in the figure, a noticeable QE degradation occurs above substrate temperatures of 79 °C for NaKSb(Cs) and 63 °C for KCsSb.

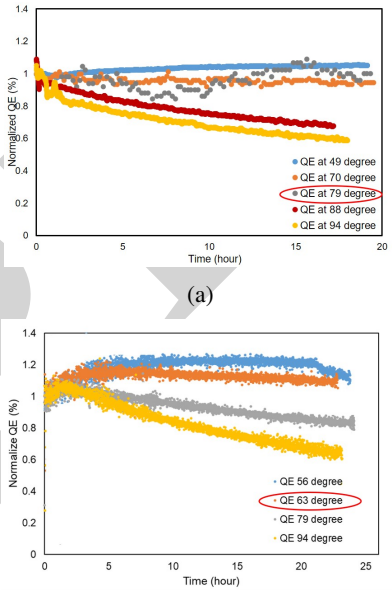

Figure 3: Decay curves of (a) NaKSb(Cs) and (b) KCsSb (thin) photocathodes measured at different substrate temperatures.

The $1/e$ lifetime for each measurement was obtained by fitting the QE decay curves with a single exponential function, $\mathrm{QE}(t) = \mathrm{QE}_0 e^{-t/\tau_1}$, where QE is the quantum efficiency at time t, QE_0 is the initial quantum efficiency, and τ_1 is the decay time constant. Table 1 summarizes the $1/e$ lifetime of the photocathodes at different substrate temperatures. As shown in the table, the NaKSb(Cs) photocathode exhibits a significantly longer lifetime than KCsSb. At 79 °C, the lifetime exceeds 1000 hours for NaKSb(Cs), compared to 103 hours for KCsSb, and a similar trend is observed at higher temperatures. These results indicate that the NaKSb(Cs) photocathode possesses superior thermal stability compared to the KCsSb photocathode.

Table 1: Lifetime of NaKSb(Cs) and KCsSb photocathodes at different decay temperatures.

Temperature [°C]	Lifetime of NaKSb(Cs) [hours]	Lifetime of KCsSb [hours]
79	> 1000	103
94	42	38
103	28	22

Spectral Reflectivity Analysis During Thermal Degradation

Based on our previous results, the spectral reflectivity peaks are understood to originate primarily from the electronic structure of the photocathode material [7, 13]. Therefore, we investigated the evolution of the spectral reflectivity during the thermal degradation study to assess the temperature-dependent stability of the electronic structure. Figure 4 compares the spectral reflectivity of NaKSb(Cs) and KCsSb photocathodes measured at different substrate temperatures. In each case, the spectral reflectivity was recorded after the QE decay measurement.

For the NaKSb(Cs) photocathode, the spectral reflectivity pattern remains largely unchanged up to 130 °C, beyond which a notable modification in the pattern is observed (Fig. 4a). Similarly, the KCsSb photocathode exhibits no significant change in the spectral reflectivity up to 103 °C; however, beyond this temperature, the reflectivity profile undergoes considerable deformation (Fig. 4b). Such changes in the reflectivity spectra suggest a modification of the electronic structure, likely caused by thermal dissociation or structural changes within the photocathode material. Reflectivity analysis thus confirms that the electronic structure of NaKSb(Cs) remains stable up to 130 °C, compared to 103 °C for KCsSb, demonstrating the superior thermal stability of the electronic structure in NaKSb(Cs) relative to KCsSb.

A notable observation emerges when comparing the spectral reflectivity evolution with the QE decay curves presented in Fig. 3. As previously mentioned, the QE begins to degrade above 79 °C for NaKSb(Cs) and above 63 °C for KCsSb, whereas the spectral reflectivity pattern shows no significant change until 130 °C for NaKSb(Cs) and 103 °C for KCsSb (Fig. 4). This disparity might suggest that the initial QE degradation is primarily driven by the desorption of unreacted or excess Cs from the photocathode surface or from grain boundaries, rather than by structural modification of the bulk material. Since the bulk electronic structure remains intact at these temperatures, no significant change in the spectral reflectivity pattern is observed, while the QE loss is attributed to the reduction in surface Cs coverage [14].

Cs Rejuvenation Effect in NaKSb(Cs)

During the thermal degradation study, the NaKSb(Cs) photocathode was heated to 111 °C and maintained at this temperature for approximately 24 hours, after which a decrease in QE was observed across the measured wavelength range. The corresponding spectral response is shown in Fig. 5. As mentioned in the previous section, this reduction

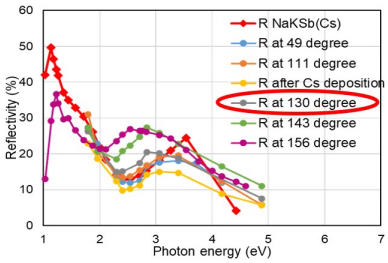

(a)

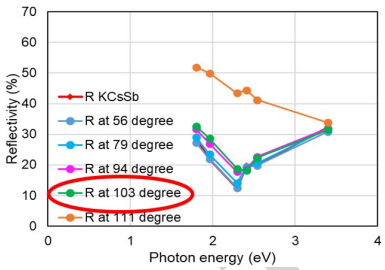

(b)

Figure 4: Spectral reflectivity of (a) NaKSb(Cs) and (b) KCsSb (thin) photocathodes measured after thermal treatment at different substrate temperatures. For the KCsSb photocathode, the spectral reflectivity was measured in the wavelength range from 365 nm to 690 nm due to experimental constraints.

in QE is attributed to Cs desorption from the photocathode structure. To restore the QE, a few nanometers of Cs were subsequently deposited onto the cathode surface, after which the QE recovered to nearly its original value, demonstrating effective rejuvenation of the photocathode (Fig. 5).

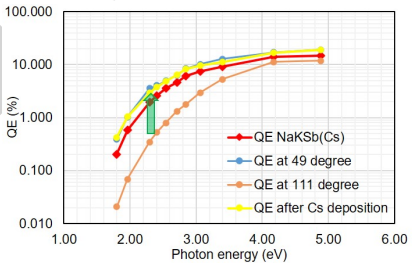

Figure 5: Spectral response of the NaKSb(Cs) photocathode at different stages of the thermal degradation study. The yellow curve corresponds to the spectral response after Cs rejuvenation.

CONCLUSION

This work summarizes the growth procedure and characterization of the NaKSb(Cs) photocathode and presents a comparative thermal degradation study with KCsSb. The results demonstrate that NaKSb(Cs) exhibits superior thermal stability compared to KCsSb. Furthermore, spectral reflectivity analysis indicates that the initial QE degradation in both photocathodes is primarily attributed to the reduction in surface Cs coverage, rather than a structural modification of the bulk material.

REFERENCES

[1] B. E. Carlsten *et al.*, "New source technologies and their impact on future light sources", *Nucl. Instrum. Methods Phys. Res. A*, vol. 622, no. 3, pp. 657–668, 2010. doi:10.1016/j.nima.2010.06.100

[2] S. Mohanty *et al.*, "Development and test results of multi-alkali antimonide photocathodes in the high gradient RF gun at PITZ", in *Proc. FEL'22*, Trieste, Italy, Aug. 2022, pp. 163–167. doi:10.18429/JACoW-FEL2022-TUP04

[3] A. di Bona *et al.*, "Development, operation and analysis of bialkali antimonide photocathodes for high-brightness photoinjectors", *Nucl. Instrum. Methods Phys. Res. A*, vol. 385, no. 3, pp. 385–390, 1997. doi:10.1016/S0168-9002(96)00809-1

[4] S. Mohanty *et al.*, "Development and operational performance of multi-alkali antimonide photocathodes", in *Proc. IPAC'25*, Taipei, Taiwan, Jun. 2025, pp. 1578–1581. doi:10.18429/JACoW-IPAC2025-TUPS067

[5] K. Kruppa *et al.*, "High Precision Temperature Control of Normal-conducting RF GUN for a High Duty Cycle Free-Electron Laser", in *Proc. 5th Int. Conf. Simulation and Modeling Methodologies, Technologies and Applications (SIMULTECH)*, Colmar, France, 2015, pp. 307–317. doi:10.5220/0005567503070317

[6] S. K. Mohanty *et al.*, "Development of Multi-Alkali Antimonides Photocathodes for High-Brightness RF Photoinjectors", in *Proc. IPAC'21*, Campinas, Brazil, Aug. 2021, pp. 1416–1419. doi:10.18429/JACoW-IPAC2021-TUPAB034

[7] S. Mohanty, "Development of Multi-Alkali Antimonide Photocathodes for High-Brightness RF Photoinjectors", Ph.D. thesis, University of Hamburg, Hamburg, Germany, 2024, p. 333. doi:10.3204/PUBDB-2024-07054

[8] L. Monaco *et al.*, "Photocathode activities at INFN LASA", in *Proc.IPAC'23*, Venice, Italy, May 2023, pp. 1370–1373. doi:10.18429/JACoW-IPAC2023-TUPA008

[9] E. D. Palik, "Introductory Remarks", in *Handbook of Optical Constants of Solids*, Elsevier, 1985, pp. 3–9. doi:10.1016/b978-0-08-054721-3.50006-x

[10] W. E. Spicer, "Photoemissive, Photoconductive, and Optical Absorption Studies of Alkali-Antimony Compounds", *Phys. Rev.*, vol. 112, no. 1, pp. 114–122, Oct. 1958. doi:10.1103/PhysRev.112.114

[11] W. H. McCarroll, R. J. Paff, and A. H. Sommer, "Role of Cs in the (Cs)Na_2KSb (S-20) Multialkali Photocathode", *J. Appl. Phys.*, vol. 42, no. 2, pp. 569–572, 1971. doi:10.1063/1.1660065

[12] A. Natarajan, A. T. Kalghatgi, B. M. Bhat, and M. Satyam, "Role of the cesium antimonide layer in the Na_2KSb/Cs_3Sb photocathode", *J. Appl. Phys.*, vol. 90, pp. 6434–6439, 2001. doi:10.1063/1.1413943

[13] S. K. Mohanty *et al.*, "Development and Characterization of Multi-Alkali Antimonide Photocathodes for High-Brightness RF Photoinjectors", *Micromachines*, vol. 14, no. 6, p. 1182, May 2023. doi:10.3390/mi14061182

[14] Z. Ding *et al.*, "Temperature-dependent quantum efficiency degradation of K-Cs-Sb bialkali antimonide photocathodes grown by a triple-element codeposition method", *Phys. Rev. Accel. Beams*, vol. 20, p. 113401, Nov. 2017. doi:10.1103/PhysRevAccelBeams.20.113401